Electron-impact excitation cross sections for Fe^{16+} in the configuration-average distorted-wave approximation

M. S. Pindzola and S. D. Loch
Department of Physics, Auburn University, Auburn, Alabama 36849, USA

C. P. Ballance and D. C. Griffin
Department of Physics, Rollins College, Winter Park, Florida 32789, USA

(Received 28 October 2005; published 27 January 2006)

Electron-impact excitation cross sections for the $2p^6 \rightarrow 2p^5 3l$ transitions in Fe^{16+} are calculated in a configuration-average distorted-wave approximation. Resonant-excitation contributions from the $2p^5 3pnl'$, $2p^5 3dnl'$, and $2p^5 4lnl'$ series are included in the isolated resonance approximation. The accuracy of the distorted-wave calculations is determined by comparison with previous 139 level resolved ($n \leqslant 5$) fully relativistic *R*-matrix calculations. Excellent agreement is found between the configuration-average distorted-wave and *R*-matrix total rate coefficients for the strong $2p^6 \rightarrow 2p^5 3p$ and $2p^6 \rightarrow 2p^5 3d$ transitions, while differences found for the relatively weak $2p^6 \rightarrow 2p^5 3s$ transition are mainly attributed to close-coupling effects.

DOI: 10.1103/PhysRevA.73.012718 PACS number(s): 34.50.Fa

Electron-impact excitation is the main excited state population mechanism leading to line emission for most astrophysical and laboratory plasmas. For inertial and magnetically confined fusion plasmas, a better understanding of the spectral emission of moderately charged heavy atomic ions has become quite important. The hohlraum for indirect drive laser fusion is typically made of gold [1], while tungsten [2] is a serious option for divertor plasma facing components in future large tokamaks. The excitation cross sections and rate coefficients for atomic ions with outer *s* and *p* subshells can generally be determined using the nonperturbative *R*-matrix method [3]. The close-coupling expansion in the *R*-matrix method is either *LS* term, *LSJ* level, or *jjJ* level resolved for the ground and low-lying excited states and includes contributions from resonant-excitation in a natural way. However, for atomic ions involving outer *d*, *f*, or even *g* subshells, the number of term or level resolved states in the close-coupling expansion may become prohibitively large. On the other hand, excitation cross sections and rate coefficients for heavy atomic ions involving $l \geqslant 2$ outer subshells may be readily calculated using a perturbative distorted-wave method [4], in which the states are only resolved as to configuration, and contributions from resonant excitation may be easily included. However, it is important to better understand the overall accuracy of the configuration-average distorted-wave method for the excitation of atomic ions.

Previously [5], electron-impact excitation cross sections calculated in the configuration-average distorted-wave approximation have been found to be in good agreement with electron-beam ion-trap (EBIT) experiments [6] for the $2s \rightarrow 3p$ transition in Fe^{23+}. Once folded with a 35 eV Gaussian energy distribution, the theoretical resonance structures were found to line up well with the EBIT measurements. In this paper we further check the accuracy of the configuration-average distorted-wave method by comparison to fully relativistic *R*-matrix calculations [7] for the $2p^6 \rightarrow 2p^5 3l$ transitions in Fe^{16+}. By summing over final levels, the *jjJ* level resolved *R*-matrix cross sections are converted to configuration only resolution. Of particular interest is the comparison between the two different theoretical resonance structures. Once folded over a Maxwellian energy distribution, the configuration-average distorted-wave and *R*-matrix rate coefficients are compared to ascertain the level of accuracy to be expected from the distorted-wave method in various plasma applications.

The general $I \rightarrow F$ transition between configurations is of the form;

$$(n_1 l_1)^{w_1+1} (n_2 l_2)^{w_2-1} k_i l_i \rightarrow (n_1 l_1)^{w_1} (n_2 l_2)^{w_2} k_f l_f, \qquad (1)$$

where $n_1 l_1$ and $n_2 l_2$ are quantum numbers of the bound electrons and $k_i l_i$ and $k_f l_f$ are quantum numbers of the initial and final continuum electrons. The direct excitation cross section is given by [4]

$$\sigma_{direct}(I \rightarrow F) = \frac{8\pi}{k_i^3 k_f}(w_1 + 1)(4l_2 + 3 - w_2) \times \sum_{l_i, l_f} (2l_i + 1)(2l_f + 1)|M(I \rightarrow F)|^2, \qquad (2)$$

where the scattering matrix element $M(I \rightarrow F)$ is a sum over products of standard angular factors and radial electrostatic integrals. Using the isolated resonance approximation and the principle of detailed balance, the indirect resonant-excitation cross section is given by [4]

$$\sigma_{indirect}(I \rightarrow F) = \frac{2\pi^2}{\Delta \epsilon k_i^2} \sum_J \frac{G_J}{2G_I} \frac{A_a(J \rightarrow I) A_a(J \rightarrow F)}{\sum_N A_a(J \rightarrow N) + \sum_{N'} A_r(J \rightarrow N')}, \qquad (3)$$

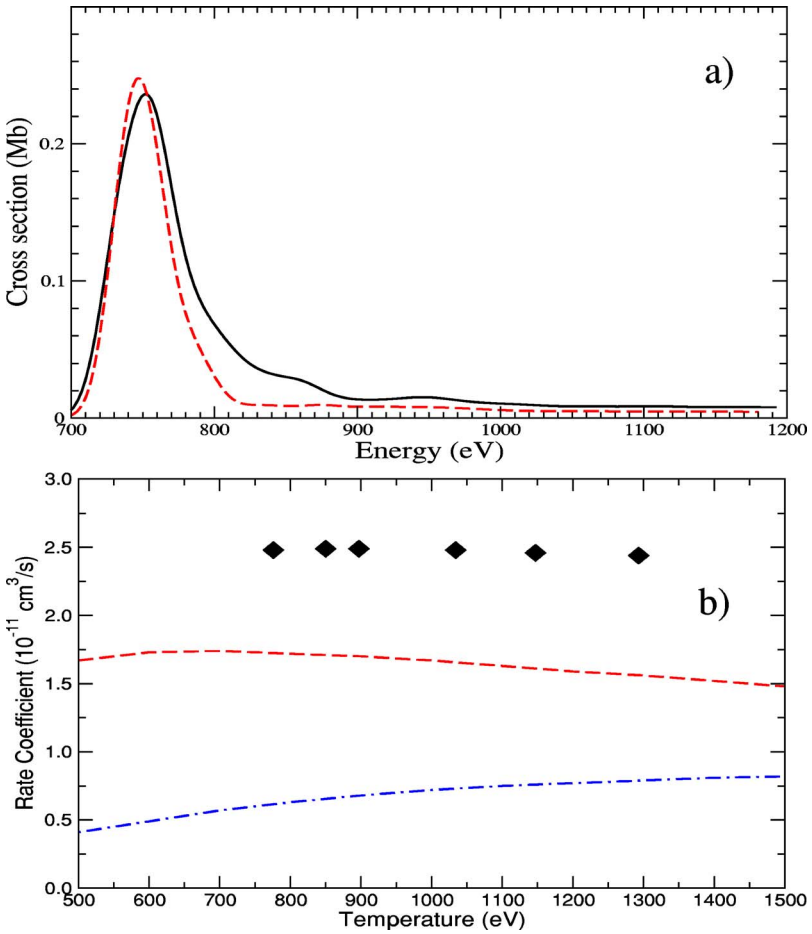

FIG. 1. (Color online) The $2p^6 \rightarrow 2p^5 3s$ transition in Fe^{16+}. (a) Cross section convoluted with a 30 eV Gaussian energy distribution. Solid line—configuration-average R-matrix calculations; dashed line—configuration-average distorted-wave calculations. (b) Maxwellian rate coefficient. Solid diamonds—configuration-average R-matrix calculations; dashed line—configuration-average distorted-wave calculations; dot-dash line—background configuration-average distorted-wave calculations (1.0 Mb$=1.0\times10^{-18}$ cm^2).

where $\Delta\epsilon$ is an energy bin width larger than the largest resonance width and G_I is the statistical weight of configuration I. The configuration-average autoionization, A_a, and radiative, A_r, rates are found in terms of products of standard angular factors and radial electrostatic and dipole integrals, respectively. The energies and bound orbitals needed to evaluate the cross sections of Eqs. (2) and (3) are calculated in the Hartree-Fock relativistic (HFR) approximation [8], which includes the mass velocity and Darwin corrections within modified HF differential equations. The continuum radial orbitals are obtained by solving a single-channel Schrödinger equation, which also includes the mass velocity and Darwin corrections, where the distorting potential is constructed from HFR bound orbitals.

Configuration-average distorted-wave and R-matrix cross sections and rate coefficients for the $2p^6 \rightarrow 2p^5 3l$ transitions in Fe^{16+} are shown in Figs. 1–3. The cross sections are convoluted with a 30 eV Gaussian energy distribution for direct comparison with future EBIT experimental measurements. The rate coefficients are obtained using a standard Maxwellian energy distribution.

For the $2p^6 \rightarrow 2p^5 3s$ transition shown in Fig. 1, the distorted-wave cross sections and rate coefficients include indirect resonant-excitation contributions from the $2p^5 3pnl'$, $2p^5 3dnl'$, and $2p^5 4lnl'$ resonance series. The $2p^5 3dnl'$ resonances, starting at $n=7$, dominate the indirect contributions. The fully relativistic R-matrix calculations included 139 jjJ levels in the $n \leqslant 5$ close-coupling expansion [7], and thus include indirect resonant-excitation contributions from the levels associated with the $2p^5 3lnl'$, $2p^5 4lnl'$, and $2p^5 5lnl'$ configurations. By comparison with previous semirelativistic R-matrix calculations which included 89 LSJ levels in an $n \leqslant 4$ close-coupling expansion [9], the $2p^5 5lnl'$ indirect resonant-excitation contributions were found to be quite small. The configuration-average R-matrix cross sections and rate coefficients are obtained by summing over the 4 jjJ levels in the final $2p^5 3s$ configuration. The distorted-wave and R-matrix convoluted cross sections found in Fig. 1(a) are in reasonable agreement as to the size and shape of the large resonance contribution near threshold. However, the distorted-wave rate coefficient found in Fig. 1(b) is about 30% below the R-matrix rate coefficient over a wide temperature range. Most of the difference may be attributed to the fact that the background R-matrix cross section is about 5/3 times the background distorted-wave cross section, due to the close-coupling of the weak $2p^6 \rightarrow 2p^5 3s$ transition with the strong $2p^6 \rightarrow 2p^5 3p$ and $2p^6 \rightarrow 2p^5 3d$ transitions. Since the Maxwellian distribution "samples" the cross section over a wide energy range, what looks like a negligible background on a cross section plot can still make important differences on a rate coefficient plot. Some of the difference may also be attributed to different resonance positions, interacting resonance effects, and radiation damping.

For the $2p^6 \rightarrow 2p^5 3p$ transition shown in Fig. 2, the

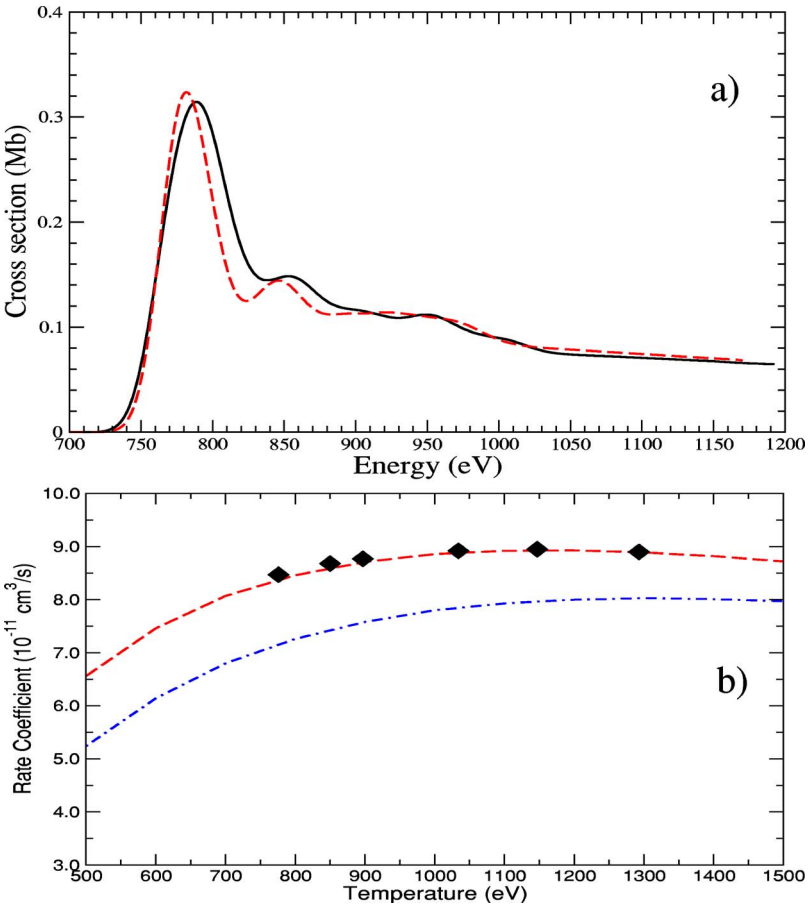

FIG. 2. (Color online) The $2p^6 \rightarrow 2p^5 3p$ transition in Fe^{16+}. (a) Cross section convoluted with a 30 eV Gaussian energy distribution. Solid line—configuration-average R-matrix calculations; dashed line—configuration-average distorted-wave calculations. (b) Maxwellian rate coefficient. Solid diamonds—configuration-average R-matrix calculations; dashed line—configuration-average distorted-wave calculations; dot-dash line—background configuration-average distorted-wave calculations (1.0 Mb$=1.0\times10^{-18}$ cm^2).

distorted-wave cross sections and rate coefficients include resonant-excitation contributions from the $2p^5 3dnl'$ and $2p^5 4lnl'$ resonance series. The $2p^5 3dnl'$ resonances, starting at $n=10$, dominate the indirect contributions. The configuration-average R-matrix cross sections and rate coefficients are obtained by summing over the 10 jjJ levels in the final $2p^5 3p$ configuration. The distorted-wave and R-matrix convoluted cross sections found in Fig. 2(a) are in reasonable agreement as to the size and shape of the resonance features, while the distorted-wave and R-matrix rate coefficients found in Fig. 2(b) are in excellent agreement. We note that the background R-matrix cross section is approximately equal to the background distorted-wave cross section.

For the $2p^6 \rightarrow 2p^5 3d$ transition shown in Fig. 3, the distorted-wave cross sections and rate coefficients include resonant-excitation contributions from only the $2p^5 4lnl'$ resonance series. The configuration-average R-matrix cross sections and rate coefficients are obtained by summing over the 12 jjJ levels in the final $2p^5 3d$ configuration. The distorted-wave and R-matrix convoluted cross sections found in Fig. 3(a) are in reasonable agreement as to the size and shape of the resonance features, while the distorted-wave and R-matrix rate coefficients found in Fig. 3(b) are in excellent agreement. We note that the background R-matrix cross section is approximately equal to the background distorted-wave cross section.

In summary, configuration-average distorted-wave calculations for the $2p^6 \rightarrow 2p^5 3l$ transitions in Fe^{16+} yield total electron-impact excitation cross sections, including both direct excitation and indirect resonant-excitation contributions, that are in reasonable agreement with recent nonperturbative fully relativistic R-matrix calculations [7]. Both the distorted-wave and R-matrix calculations find that the $2p^6 \rightarrow 2p^5 3s$ transition is an order of magnitude weaker than the $2p^6 \rightarrow 2p^5 3d$ transition, while the $2p^6 \rightarrow 2p^5 3p$ transition is a factor of three smaller than the $2p^6 \rightarrow 2p^5 3d$ transition. The strong resonance enhancement of the $2p^6 \rightarrow 2p^5 3s$ transition is mainly due to $n \geqslant 7$ resonances attached to the $2p^5 3d$ configuration, while the resonance enhancement of the $2p^6 \rightarrow 2p^5 3p$ transition is mainly due to $n \geqslant 10$ resonances attached to the same $2p^5 3d$ configuration. Excellent agreement is found between the configuration-average distorted-wave and R-matrix rate coefficient calculations for the strong $2p^6 \rightarrow 2p^5 3p$ and $2p^6 \rightarrow 2p^5 3d$ transitions, while the 30% shortfall in the distorted-wave versus R-matrix rate coefficients for the weak $2p^6 \rightarrow 2p^5 3s$ transition is mainly attributed to close-coupling effects on the background direct excitation cross section. Thus, it appears that the overall accuracy of a configuration-average distorted-wave method, that includes both direct excitation and indirect resonant-excitation contributions, can be quite good for the electron-impact excitation of atomic ions. Although more comparisons with nonperturbative R-matrix calculations and experimental measurements are always welcome, we think that the application

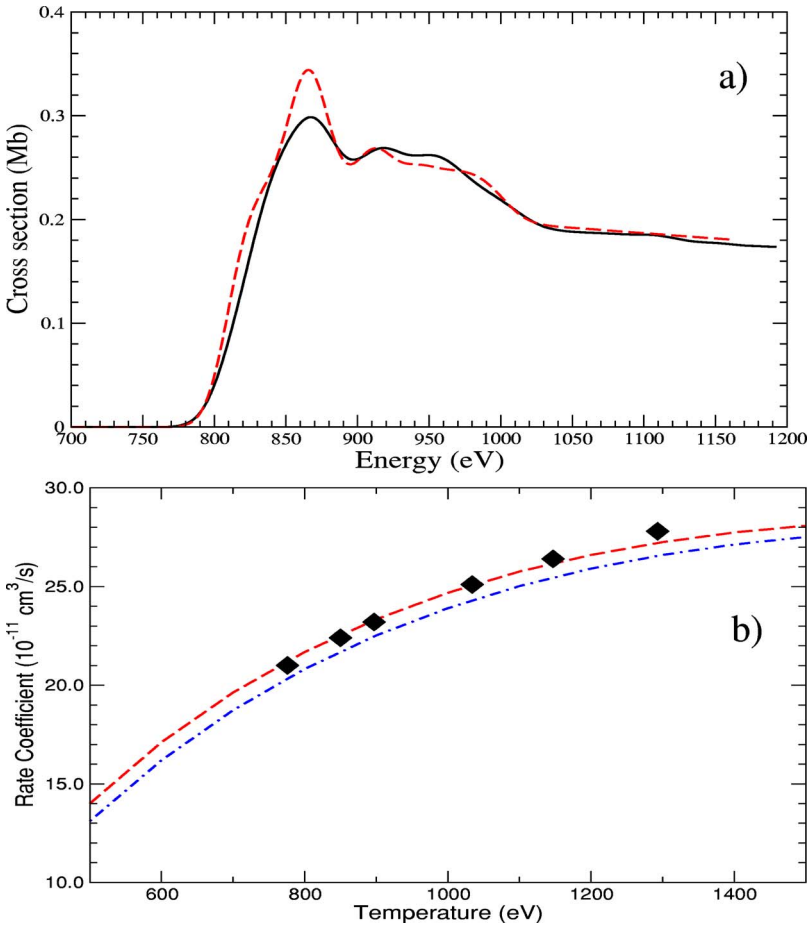

FIG. 3. (Color online) The $2p^6 \rightarrow 2p^5 3d$ transition in Fe^{16+}. (a) Cross section convoluted with a 30 eV Gaussian energy distribution. Solid line—configuration-average *R*-matrix calculations; dashed line—configuration-average distorted-wave calculations. (b) Maxwellian rate coefficient. Solid diamonds—configuration-average *R*-matrix calculations; dashed line—configuration-average distorted-wave calculations; dot-dash line—background configuration-average distorted-wave calculations (1.0 Mb$=1.0\times10^{-18}$ cm^2).

of the configuration-average distorted-wave method to electron-impact excitation processes in the complex heavy metal ions seen in controlled fusion plasmas is a promising way forward.

This work was supported in part by grants from the U.S. Department of Energy. Computational work was carried out at the National Energy Research Scientific Computing Center in Oakland, California.

[1] M. J. May, P. Beiersdorfer, M. Schneider, S. Terracol, K. L. Wong, K. Fournier, B. Wilson, J. H. Scofield, K. J. Reed, G. Brown, F. S. Porter, R. Kelley, C. A. Kilbourne, and K. R. Boyce, in *Atomic Processes in Plasmas*, edited by J. S. Cohen, S. Mazevet, and D. P. Kilcrease, AIP Conf. Proc. No. 730 (AIP, New York, 2004), p. 61.

[2] R. Neu, R. Dux, A. Kallenbach, T. Putterich, M. Balden, J. C. Fuchs, A. Herrmann, C. F. Maggi, M. O'Mullane, R. Pugno, I. Radivojevic, V. Rohde, A. C. C. Sips, W. Suttrop, A. Whiteford, and the ASDEX Upgrade Team, Nucl. Fusion **45**, 209 (2005).

[3] *Atomic and Molecular Processes: An R-matrix Approach*, edited by P. G. Burke and K. A. Berrington (IOP, London, 1993).

[4] M. S. Pindzola, D. C. Griffin, and C. Bottcher, in *Atomic Processes in Electron-Ion and Ion-Ion Collisions*, edited by F. Brouillard, NATO ASI Ser., Ser. B (Plenum, New York, 1986), Vol. **145**, p. 75.

[5] M. S. Pindzola, Phys. Rev. A **65**, 014701 (2001).

[6] M. F. Gu, S. M. Kahn, D. W. Savin, P. Beiersdorfer, G. V. Brown, D. A. Liedahl, K. J. Reed, C. P. Bhalla, and S. R. Grabbe, Astrophys. J. **518**, 1002 (1999).

[7] S. D. Loch, M. S. Pindzola, C. P. Ballance, and D. C. Griffin, J. Phys. B **39**, 85 (2006).

[8] R. D. Cowan, *The Theory of Atomic Structure and Spectra* (University of California Press, Berkeley, 1981).

[9] G. X. Chen and A. K. Pradhan, Phys. Rev. Lett. **89**, 013202 (2002).